Effect of reactive surface area of minerals on mineralization trapping of CO_2 in saline aquifers

LUO Shu, XU Ruina and JIANG Peixue*

Key Laboratory for Thermal Science and Power Engineering of Ministry of Education, Beijing Key Laboratory of CO_2 Utilization and Reduction Technology, Department of Thermal Engineering, Tsinghua University, Beijing 100084, China

Abstract: The reactive surface area, an important parameter controlling mineral reactions, affects the amount of mineralization trapping of CO_2 which affects the long-term CO_2 storage. The effect of the reactive surface area on the mineralization trapping of CO_2 was numerically simulated for CO_2 storage in saline aquifers. Three kinds of minerals, including anorthite, calcite and kaolinite, are involved in the mineral reactions. This paper models the relationship between the specific surface area and the grain diameter of anorthite based on experimental data from literature (Brantley and Mellott, 2000). When the reactive surface areas of anorthite and calcite decrease from 838 to 83.8 m^2/m^3, the percentage of mineralization trapping of CO_2 after 500 years decreases from 11.8% to 0.65%. The amount of dissolved anorthite and the amounts of precipitated kaolinite and calcite decrease significantly when the reactive surface areas of anorthite and calcite decrease from 838 to 83.8 m^2/m^3. Calcite is initially dissolved in the brine and then precipitates during the geochemical reactions between CO_2-H_2O and the minerals. Different reactive surface areas of anorthite and calcite lead to different times from dissolution to precipitation. The pH of the brine decreases with decreasing reactive surface areas of anorthite and calcite which influences the acidity of the saline aquifer. The gas saturation between the upper and lower parts of the saline aquifer increases with decreasing reactive surface areas of anorthite and calcite. The mass density distribution of brine solution shows that the CO_2+brine solution region increases with decreasing reactive surface areas of anorthite and calcite.

Key words: Reactive surface area, mineralization trapping, dissolution; precipitation, brine mass density, CO_2 geological storage

1 Introduction

Greenhouse gas emissions especially CO_2 emissions have become a critical environmental issue and the reduction of CO_2 emissions is now a global concern. Various approaches have been developed to reduce CO_2 emissions, including developing renewable energy source (Mohibullah and Imtiaz, 2006), increasing energy efficiency (Markus et al, 2007) and carbon dioxide capture and storage (CCS) (IPCC, 2005). CCS has great potential for large-scale CO_2 disposal. Geological CO_2 storage in saline aquifers has the greatest CO_2 storage potential due to its large capacity and proximity to CO_2 emission sources. Tore and Gale (2004) reported the first CO_2 geological storage demonstration project.

Full-field simulations of CO_2 geological storage have been used to evaluate the storage capacity and injection issues. A variety of simulators have been developed by the petroleum industry (Johnson et al, 2005), including ECLIPSE (Exploration Consultants Limited Implicit Program for Simulation Engineering), TOUGH (Transport of Unsaturated Groundwater and Heat), NUFT (Nonisothermal, Unsaturated Flow and Transport) and CMG-GEM (Canada Modeling Group-Generalized Equation of State Model), for numerical simulation study. Asghari et al (2006) used CMG-GEM for investigating the effect of the operating parameters on the CO_2 storage capacity in a heterogeneous oil reservoir, and found that a combination of two vertical injection wells and one horizontal production well will give the optimal storage capacity. After being injected into saline aquifers, CO_2 is trapped by four trapping mechanisms, namely structural trapping, residual trapping, solubility trapping and mineral trapping (IPCC, 2005; Yang, 2010). The simulators mentioned above are used to model the movement of the CO_2 plume, the flow characteristics and the rate of the four trapping mechanisms during and after CO_2 injection. Mineralization trapping is assumed to be permanent (IPCC, 2005).

Several researchers have investigated the trapping mechanisms to evaluate the storage capacity and the leakage risk of CO_2 geological storage projects (Doughty, 2010). Nghiem et al (2004; 2005) used an advanced geochemical equation of state (EOS) compositional simulator (GEM) to

numerically simulate the complex process associated with CO_2 enhanced oil recovery (CO_2 EOR), CO_2 storage and CO_2 enhanced coal bed methane (CO_2 ECBM) processes. Basbug and Gumrah (2005) used software CMG-GEM for studying the ability of aquifers to capture CO_2 injected in a supercritical state for a long period of time (200 years). Frangeul et al (2004) used CMG-GEM for evaluating long term migration of CO_2 in the Sleipner/Utsira CO_2 geological storage project. Thibeau and Nghiem (2007) modelled the CO_2 mineralization process, taking various possible reactions into consideration. Shekhar et al (2006) conducted numerical simulation of geochemical processes with fluid flow and seismic models.

Many parameters can influence the CO_2 plume and flow characteristics, including temperature, pressure, permeability, aquifer dip angle and heterogeneity. Kumar et al (2004) investigated the effects of the average permeability, the vertical to horizontal permeability ratio, the residual gas saturation, salinity, temperature, aquifer dip angle and permeability heterogeneity on CO_2 geological storage. Green and King (2010) studied the effect of the vertical heterogeneity on long-term migration of CO_2 in saline formations. Ozah et al (2005) investigated the influences of heterogeneity, dip angle and the vertical to horizontal permeability ratio on the storage potential and injection of a CO_2-H_2S gas mixture. Bryant et al (2006) studied the buoyancy dominated multiphase flow and its effect on CO_2 geological storage. Doughty (2007) investigated the influence of the relative permeability hysteresis on CO_2 geological storage using TOUGH2. Juanes et al (2006) investigated the effect of the relative permeability hysteresis on CO_2 geological storage, and the results showed the importance of the relative permeability model for predicting the distribution and the migration of CO_2 in the formation. The effects of the residual gas and water saturation, hysteresis and permeability anisotropy on CO_2 distribution between the gaseous and aqueous phases were investigated (Ukaegbu et al, 2009). Saadatpoor et al (2007) studied the effect of heterogeneity distribution of the capillary pressure curve on a buoyancy driven CO_2 plume. Chang and Bryant (2007) investigated the effect of faults on the buoyancy driven CO_2 plume and the residual CO_2 trapping.

The effect of reactive surface area of minerals on CO_2 geological storage has rarely been reported. Most researchers used a constant reactive surface area of minerals to simulate CO_2 geological storage. However, as one important parameter controlling the mineral reactions, the reactive surface area of minerals affects the level of mineralization trapping of CO_2 and long-term CO_2 storage. In this study, the effect of the reactive surface area of anorthite and calcite on mineralization trapping of CO_2 in saline aquifers was investigated by using the software CMG-GEM.

2 Model description

2.1 Geometric model and geochemical reactions

The 2D model developed with CMG (shown in Fig. 1) was used to investigate the effect of the reactive surface areas of anorthite and calcite on the mineralization trapping of CO_2.

The static grid model parameters and reservoir parameters are given in Table 1. The injection well perforation location was at the left bottom. The geochemical reactions between the gaseous and aqueous phases and between aqueous and solid phases are the following four solubility reactions and three liquid-mineral reactions:

$$CO_2(aq) + H_2O \Leftrightarrow H^+ + HCO_3^- \tag{1}$$
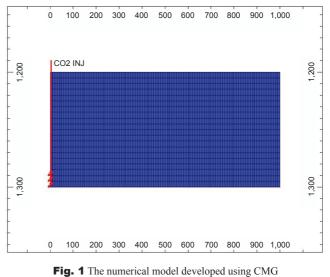
$$CO_2(aq) + H_2O \Leftrightarrow H^+ + HCO_3^- \tag{2}$$

$$HCO_3^- \Leftrightarrow H^+ + CO_3^{2-} \tag{3}$$

$$H_2O \Leftrightarrow H^+ + OH^- \tag{4}$$

$$Calcite + H^+ \Leftrightarrow Ca^{2+} + HCO_3^- \tag{5}$$

$$Anorthite + 8H^+ \Leftrightarrow Ca^{2+} + 2Al^{3+} + 2SiO_2(aq) + 4H_2O \tag{6}$$

$$Kaolinite + 6H^+ \Leftrightarrow 2Al^{3+} + 2SiO_2(aq) + 5H_2O \tag{7}$$

Fig. 1 The numerical model developed using CMG

Table 1 Aquifer parameters and model parameters

Aquifer size	1000m×10m×100m
Grid	100×1×20
Porosity	0.18
Permeability	100 mD
Aquifer depth	1200 m
Reservoir temperature	50 °C
Salinity (NaCl)	0.1%
Maximum injection rate	8000 m³/day (under standard surface gas state)
Injection period	1 year
Rock compressibility	5.8×10^{-7} kPa⁻¹ (at reference pressure:11800 kPa)
Water compressibility	4.5×10^{-7} kPa⁻¹ (at reference pressure:13100 kPa)

The minerals in the geochemical reactions are calcite, anorthite and kaolinite. The gaseous CO_2 fugacity (f_{g,CO_2}) was calculated using the Peng-Robinson equation of state. The aqueous CO_2 fugacity (f_{aq,CO_2}) is the same as the gaseous CO_2 fugacity. The CO_2 mole fraction in the aqueous phase y_{aq,CO_2} was calculated by Henry's law as follows:

$$f_{g,CO_2} = f_{aq,CO_2} = y_{aq,CO_2} \cdot H_{CO_2} \tag{8}$$

Henry's law constant H_{CO_2} is a function of the pressure, temperature and salinity and was calculated by using the method reported by Li and Nghiem (1986).

The mineral reaction rate was calculated by using Eq. (9) reported in literature (Bethke, 1996):

$$r_\alpha = A_\alpha k_\alpha (1 - \frac{Q_\alpha}{K_{eq,\alpha}}) \tag{9}$$

where r_a is the reaction rate, A_a is the reactive surface area, k_a is the reaction rate constant, Q_a is the mineral reaction activity product, and $K_{eq,a}$ is the chemical equilibrium constant of the mineral reaction.

2.2 Model for relative permeability

Corey's model (Corey, 1976) is used to calculate the relative permeability of CO_2 and brine during the drainage process. The relative permeability of water (K_{rw}) and the relative permeability of CO_2 (K_{rg}) versus water saturation (S_w) are shown in Fig. 2. The hysteresis effect on the relative permeability of CO_2 is modeled by using the modified Land equation which is integrated into CMG-GEM. In this paper the maximum CO_2 residual saturation is assumed to be 0.2.

3 Reactive surface area of minerals

The mineralization trapping is influenced by the reactive surface area of minerals. For a clastic rock, the reactive surface area of an individual mineral grain is dependent on the grain size. The specific surface area of anorthite with different grain diameters was measured (Brantley and Mellott, 2000). The specific surface area of kaolinite was investigated
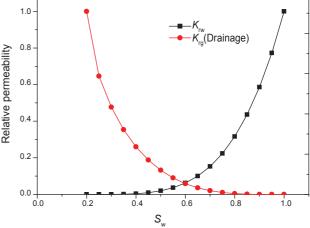

Fig. 2 Relative permeability curves versus water saturation

(Raman and Mortland, 1966). In our work, Brantley and Mellott's experimental data (Brantley and Mellott, 2000) were used to fit the relationship between the specific surface area of anorthite and its grain diameter as follows:

$$\log S = -1.19542 \log D + 8.44891 \tag{10}$$

where S is the specific surface area, D is the anorthite grain diameter.

The data and the fitting line are shown in Fig. 3. The volume fraction and the reactive surface area of calcite are assumed to be the same as those of anorthite (Nghiem et al, 2004). However, Nghiem assumed the reactive surface area was a constant. In this paper the relationship between the reactive surface area and grain diameter is investigated. This paper also assumed that the volume fraction and the reactive surface area of calcite are the same as those of anorthite. Table 2 lists the reactive surface areas of calcite and anorthite with seven grain sizes and their other parameters. The kaolinite grain diameters are assumed to be 1-2 μm with a specific surface area of $1.04 \times 10^7 \, m^2/m^3$. The kaolinite volume fraction in the saline aquifer is 1.76% and the reactive surface area is $1.83 \times 10^7 \, m^2/m^3$.

Table 2 The reactive surface areas of calcite and anorthite with different grain sizes

Case ID	Grain diameter μm	Specific surface area of Calcite, m²/m³	Specific surface area of Anorthite, m²/m³	Volume fraction of Calcite	Volume fraction of Anorthite	Reactive surface area of Calcite, m²/m³	Reactive surface area of Anorthite, m²/m³
Case 1	50	2.62×10^6	2.62×10^6	0.88%	0.88%	2.30×10^4	2.30×10^4
Case 2	100	1.14×10^6	1.14×10^6	0.88%	0.88%	1.01×10^4	1.01×10^4
Case 3	200	4.99×10^5	4.99×10^5	0.88%	0.88%	4.39×10^3	4.39×10^3
Case 4	300	3.07×10^5	3.07×10^5	0.88%	0.88%	2.71×10^3	2.71×10^3
Case 5	500	1.67×10^5	1.67×10^5	0.88%	0.88%	1.47×10^3	1.47×10^3
Case 6	800	9.52×10^4	9.52×10^4	0.88%	0.88%	838	838
Case 7	800	9.52×10^4	9.52×10^4	0.088%	0.088%	83.8	83.8

Fig. 3 The relationship of the specific surface area of anorthite and its grain diameter

Fig. 4 Quantity of supercritical CO_2 with time for anorthite and calcite with different reactive surface areas

4 Results and discussion

4.1 CO_2 trapping mechanism

When CO_2 is injected underground, the CO_2 is trapped by structural trapping, residual trapping, solubility trapping and mineral trapping. According to the four trapping mechanisms, there are three states in which CO_2 exists underground, namely supercritical CO_2 which includes free gas under caprock and the residual trapped gas, the aqueous CO_2 which is the dissolved gas, and the mineralized CO_2 which is the mineral trapped gas. The quantities of supercritical, aqueous and mineralized CO_2 with time are shown in Figs. 4-6 for seven anorthite and calcite reactive surface areas. It can be seen that quantity of the supercritical CO_2 decreases with time. The quantities of the aqueous CO_2 and mineralized CO_2 increase with time. The supercritical CO_2 quantity increases with the decrease of anorthite and calcite reactive surface areas; The aqueous CO_2 concentration increases with the decrease of anorthite and calcite reactive surface area, since the mineral-trapped CO_2 increases with the reactive surface areas of anorthite and calcite as displayed in Fig. 6, leading to less aqueous CO_2. Table 3 shows the estimated amounts of trapped CO_2 for different trapping mechanisms after 500 years. For mineral-trapped CO_2, cases 1-6 do not vary significantly. However, after 500 years, the mineralized

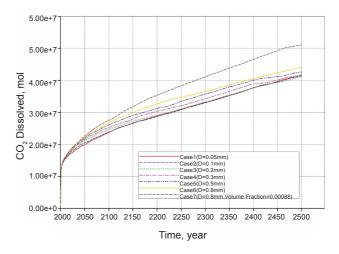**Fig. 5** Quantity of aqueous CO_2 with time for anorthite and calcite with different reactive surface areas
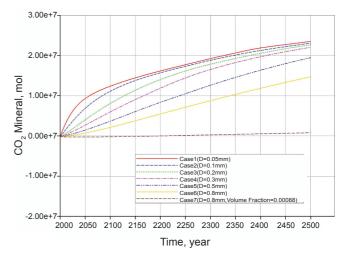

Fig. 6 Quantity of mineralized CO_2 with time for anorthite and calcite with different reactive surface areas

CO_2 decreases significantly from 11.8% to 0.65% when the anorthite and calcite reactive surface areas decrease from 838 to 83.8 m^2/m^3. The amount of free gaseous CO_2 is nearly the same for different anorthite and calcite reactive surface areas since much of CO_2 is dissolved in saline aquifers.

Table 3 The quantity of CO_2 trapped by different mechanisms after 500 years

	Residual Trapped CO_2	Dissolved CO_2	Mineralized CO_2	Free gaseous CO_2
Case 1	24.4%	33.5%	18.9%	23.2%
Case 2	22.9%	33.3%	18.5%	25.2%
Case 3	23.1%	33.0%	18.2%	25.6%
Case 4	23.8%	33.5%	17.7%	25.0%
Case 5	24.4%	34.2%	15.7%	25.7%
Case 6	25.2%	35.5%	11.8%	27.5%
Case 7	27.5%	41.1%	0.65%	30.7%

4.2 Analysis of minerals

The variations in the amounts of anorthite and kaolinite with time are shown in Figs. 7-8. The change in the amount of calcite with time is shown in Figs. 9 and 10. It can be seen that the anorthite is dissolved in the brine aquifer while the kaolinite is precipitated (Figs. 7-8); The calcite is dissolved at the beginning stage and then precipitated with time due to the continued geochemical reactions between CO_2-H_2O and the minerals (Figs. 9-10). The amount of dissolved anorthite increases with the increase of anorthite and calcite reactive surface areas, and the amounts of precipitated calcite and kaolinite also increase with the increase of anorthite and calcite reactive surface areas. The mineral reaction rate slows with time as more CO_2 reacts with the brine at the beginning of the injection as shown in Fig. 7-9. The dissolved anorthite, and the precipitated kaolinite and calcite, significantly increase as the anorthite and calcite reactive surface areas increase from 83.8 to 838 m^2/m^3 (The kaolinite grain diameters are assumed to be 1-2 μm with a specific surface area of $1.04 \times 10^7 \, m^2/m^3$. The kaolinite volume fraction in the saline aquifer is 1.76% and the reactive surface area is $1.83 \times 10^7 \, m^2/m^3$). So the mineral formation is influenced significantly by the anorthite and calcite reactive surface areas. Thus, accurate measurement of the reactive surface areas is important for assessing the long-term CO_2 geological storage and the safety of CO_2 geological storage.
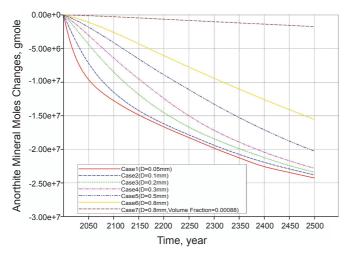

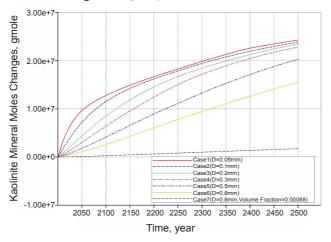**Fig. 7** The quantity of Anorthite with time

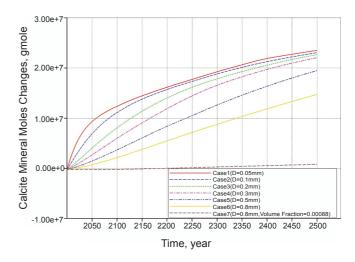**Fig. 8** The quantity of Kaolinite with time

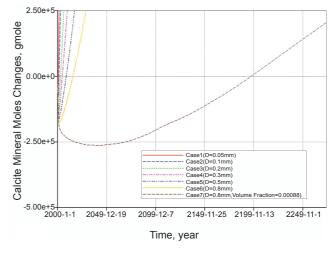**Fig. 9** The quantity of Calcite with time

Fig. 10 The quantity of Calcite with time (early stage)

4.3 Effect of volume fraction

The changes in the amounts of anorthite, calcite and kaolinite with time are shown in Figs. 11 and 12 for different volume fractions (case 6 and case 7). When the anorthite and calcite volume fractions decrease to 0.088%, the anorthite and calcite reactive surface areas decrease from 838 to 83.8 m^2/m^3. Calcite is dissolved at the beginning and then precipitated with the continued geochemical reactions between the CO_2-H_2O and the minerals. Different anorthite and calcite reactive surface areas lead to different times from dissolution to precipitation. The time becomes short with the increase of anorthite and calcite reactive surface areas, such as the conversion time of 200 years after injection for an anorthite and calcite reactive surface areas of 83.8 m^2/m^3 compared to 15 years. In addition, the amount of net precipitated calcite reflects the mineralization trapping of CO_2. Figs. 11 and 12 show that the precipitation of calcite and kaolinite increase with increasing volume fractions of calcite and anorthite. The amount of precipitated calcite for case 6 is about ten times that of case 7, which influences the long-term CO_2 geological storage significantly.
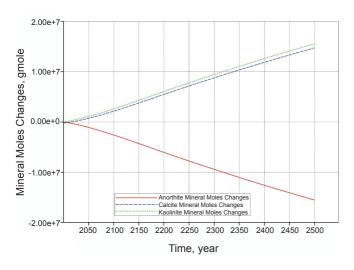
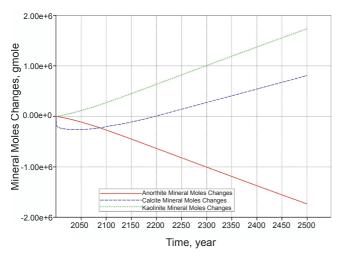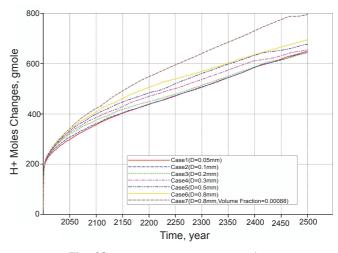**Fig. 11** Change of mineral quantities with time for case 6

Fig. 12 Change of mineral quantities with time for case 7

4.4 Gas saturation distribution

The variation in the number of H^+ moles with time which indicates the brine pH is shown in Fig. 13. The brine pH decreases with the decrease in the anorthite and calcite reactive surface areas. The dissolution of CO_2 into the brine leads to the formation of H^+ and HCO_3^-. Then lower anorthite and calcite reactive surface areas mean that less H^+ react with the minerals so there is more H^+ in the brine and the pH decreases.

The CO_2 saturation distributions for the seven cases after 500 years are shown in Figs. 14-20. The CO_2 gathering at the top part each figure is because of the structural trapping while the CO_2 gathering at the bottom part of each figure is because of the residual trapping. The gas saturation between the top and bottom parts increases with the decrease of the anorthite and calcite reactive surface areas. Larger reactive surface areas in anorthite and calcite results in quicker formation of minerals that promote the dissolving of CO_2 into the brine, leading to the disappearance of free gaseous CO_2 between the top and bottom parts. Therefore, the gas saturation between

the top and bottom parts decreases with the increase of the anorthite and calcite reactive surface areas. More CO_2 is trapped by residual trapping with less anorthite and calcite reactive surface areas due to less aqueous CO_2 reacting with the brine.
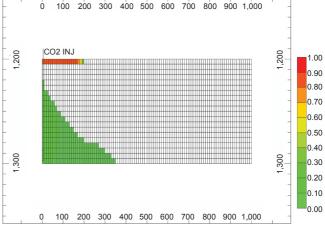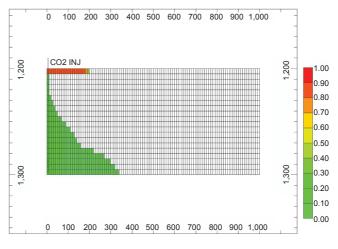

Fig. 13 The Changing in the amount of H^+

Fig. 14 CO_2 saturation for case 1

Fig. 15 CO_2 saturation for case 2

Fig. 16 CO_2 saturation for case 3

flows downwards due to gravity, promoting the upward flow of brine in the bottom part. This convection flow promotes the dissolution of CO_2 into the brine. Less carbonic acid reacts with the mineral ions when there is less anorthite and calcite reactive surface areas, leading to more carbonic acid remaining in saline aquifers. The CO_2+brine solution volume then becomes larger with less anorthite and calcite reactive surface area, which also influences the long-term geological storage of CO_2.

Fig. 19 CO_2 saturation for case 6

Fig. 17 CO_2 saturation for case 4
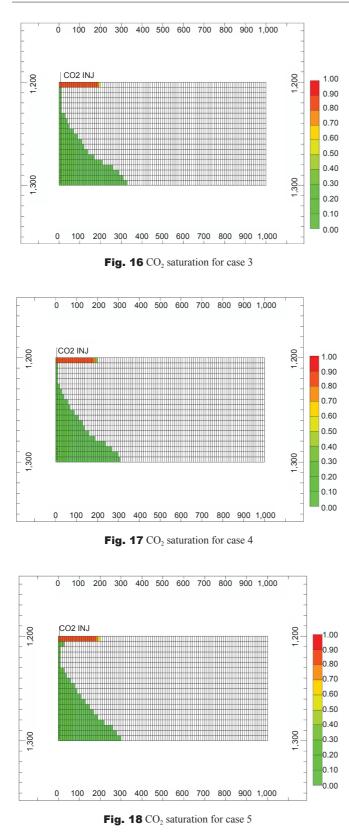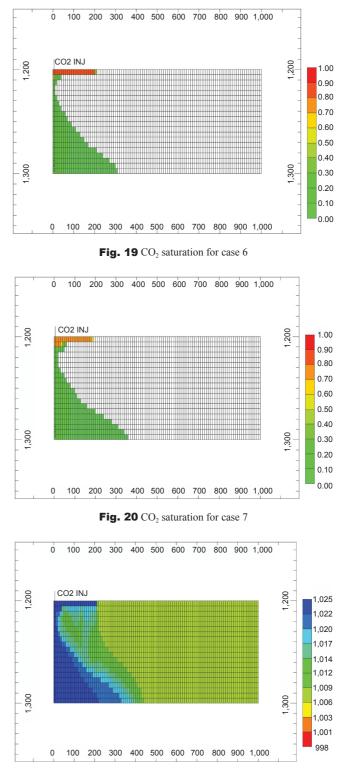

Fig. 20 CO_2 saturation for case 7

Fig. 18 CO_2 saturation for case 5

4.5 Brine mass density

The variations in brine mass density distributions for case 6 and case 7 after 500 years are shown in Figs. 21 and 22. The brine mass density is very large near the bottom. Supercritical CO_2 moves upwards due to the buoyancy effect after the CO_2 injection. Some CO_2 dissolves into the brine, which increases the brine mass density. The CO_2+brine solution then
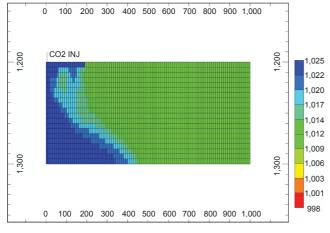

Fig. 21 The brine mass density for case 6

Fig. 22 The brine mass density for case 7

5 Conclusions

This study modelled the effect of the reactive surface areas of anorthite and calcite and the grain size on mineralization trapping of CO_2 in saline aquifers. The percentage of CO_2 stored after 500 years due to mineralization trapping decreases from 11.8% to 0.65% when the anorthite and calcite reactive surface areas reduced from 838 to 83.8 m^2/m^3. The conversion time from dissolution to precipitation of calcite is influenced by the anorthite and calcite reactive surface areas. The quantity of dissolved anorthite increases with the increase of anorthite and calcite reactive surface areas and the amounts of precipitated calcite and kaolinite also increase with the increase of anorthite and calcite reactive surface areas. The pH value decreases with the decrease of anorthite and calcite reactive surface areas which influences the brine acidity. The gas saturation between the top and bottom parts increases with the decrease of anorthite and calcite reactive surface areas. The brine mass density distribution shows that the CO_2+brine solution region becomes larger with the decrease of anorthite and calcite reactive surface areas, which influences the long-term CO_2 geological storage.

Acknowledgements

References

Asghari K, Dliwe A and Mahinpey N. Effect of operational parameters on carbon dioxide storage capacity in a heterogeneous oil reservoir: A case study. Ind. Eng. Chem. Res. 2006. 45: 2452-2456

Basbug B and Gumrah F. Simulating the effects of deep saline aquifer properties on CO_2 sequestration. 6th canadian International Petroleum Conference, Calgary, Canada. 2005

Bethke C M. Geochemical Reaction Modeling. New York: Oxford University Press. USA. 1996

Brantley S and Mellott N. Surface area and porosity of primary silicate minerals. American Mineralogist. 2000. 85: 1767-1783

Bryant S, Lakshminarasimhan S and Pope G. Buoyancy dominated multiphase flow and its impact on geological sequestration of CO_2. 2006 SPE/DOE Symposium on Improved Oil Recovery, Tulsa, USA

Chang K and Bryant S. Dynamics of CO_2 plumes encountering a fault in a reservoir. Sixth Annual Conference on Carbon Capture and Sequestration-DOE/NETL. 2007

Corey A. Mechanics of heterogeneous fluids in porous media. Water Resources Publications, Fort Collins, Colorado, USA. 1976

Doughty C. Investigation of CO_2 plume behavior for a large-scale pilot test of geologic carbon storage in a saline formation. Transp Porous Med 2010. 82: 49-76

Doughty C. Modeling geologic storage of carbon dioxide: Comparison of non-hysteretic and hysteretic characteristic curves. Energy Conversion and Management. 2007. 48: 1768-1781

Frangeul J, Nghiem L, Caroli E, et al. Sleipner/Utsira CO_2 geological storage: full field flow and geochemical coupling to assess the long term fate of the CO_2. Proceedings AAPG Annual Conference, 2004. Paper AAPG 86278

Green C and King J. Effect of vertical heterogeneity on long-term migration of CO_2 in saline formations. Trans Porous Med. 2010. 82: 31-47

IPCC. IPCC special report on carbon dioxide capture and storage. Geneva: WMO-UNEP. 2005

Johnson J, Nitao J and Morris J. Reactive transport modeling of cap rock integrity during natural and engineered CO_2 storage. Carbon Dioxide Capture for Storage in Deep Geologic Formations 2005. 2: 787-813

Juanes R, Spiteri E, Orr F, et al. Impact of relative permeability hysteresis on geological CO_2 storage. Water Resources Research. 2006. 42: W12418

Kumar A, Noh M, Pope G, et al. Reservoir simulation of CO_2 storage in deep saline aquifers. 2004 SPE/DOE Fourteenth Symposium on Improved Oil Recovery, Tulsa, USA

Li Y K and Nghiem L X. Phase equilibrium of oil, gas and water/brine mixtures from a cubic equation of state and Herry's law. Canadian Journal of Chemical Engineering. 1986. 64(3): 486-496

Markus B, Anjana D, Ulrich F, et al. Role of energy efficiency standards in reducing CO_2 emissions in Germany: An assessment with TIMES. Energy Policy 2007. 35: 772-785

Mohibullah I. and Imtiaz A. Estimation of CO_2 mitigation potential through renewable energy generation. First International Power & Energy Conference, Putrajaya, Malaysia. 2006

Nghiem L, Sammon P, Grabenstetter J, et al. Modeling CO_2 storage in aquifers with a fully-coupled geochemical EOS. 2004 SPE/DOE Fourteenth Symposium on Improved Oil Recovery, Tulsa, USA

Nghiem L, Sammon P, Kohse B, et al. Modelling CO_2 storage and CO_2 advanced recovery processes. 8th International Forum on Reservoir Simulation, Stresa, Italy. 2005

Ozah R, Lakshminarasimhan S, Pope G, et al. Numerical simulation of the storage of pure CO_2 and CO_2-H_2S gas mixtures in deep saline aquifers. 2005 SPE Annual Technical Conference and Exhibition, Dallas, USA

Raman K and Mortland M. External specific surface area of vermiculite, The American Mineralogist. 1966. 51: 1787-1792

Saadatpoor E, Bryant S and Sepehrnoori K. Effect of heterogeneity in capillary pressure on buoyancy driven flow of CO_2. Sixth Annual Conference on Carbon Capture and Sequestration-DOE/NETL. 2007

Shekhar R, Gibson R, Kumar A, et al. Seismic modeling of compositional and geochemical effects in CO_2 sequestration. SEG/New Orleans 2006 Annual Meeting

Thibeau S and Nghiem L. A modeling study of the role of selected minerals in enhancing CO_2 mineralization during CO_2 aquifer storage. 2007 SPE Annual Technical Conference and Exhibition, Anaheim, USA

Torp T and Gale J. Demonstrating storage of CO_2 in geological reservoirs: The Sleipner and SACS projects. Energy. 2004. 29: 1361-1369

Ukaegbu C, Gundogan O, Mackay E, et al. Simulation of CO_2 storage in a heterogeneous aquifer. IMechE. 2009. JPE627

Yang F, Bai B J, Tang D Z, et al. Characteristics of CO_2 sequestration in saline aquifer. Petroleum Science. 2010. 7(1): 83-92

(Edited by Zhu Xiuqin)